Photothermoelectric Effect in Suspended Semiconducting Carbon Nanotubes

Tristan DeBorde, Lee Aspitarte, Tal Sharf, Joshua W. Kevek, and Ethan D. Minot*

Department of Physics, Oregon State University, Corvallis, Oregon 97331, United States

ABSTRACT We have performed scanning photocurrent microscopy measurements of field-effect transistors (FETs) made from individual ultraclean suspended carbon nanotubes (CNTs). We investigate the spatial-dependence, polarization-dependence, and gate-dependence of photocurrent and photovoltage in this system. While previous studies of surface-bound CNT FET devices have identified the photovoltaic effect as the primary mechanism of photocurrent generation, our measurements show that photothermoelectric phenomena play a critical role in the optoelectronic properties of suspended CNT FETs. We have quantified the photothermoelectric mechanisms and identified regimes where they overwhelm the photovoltaic mechanism.

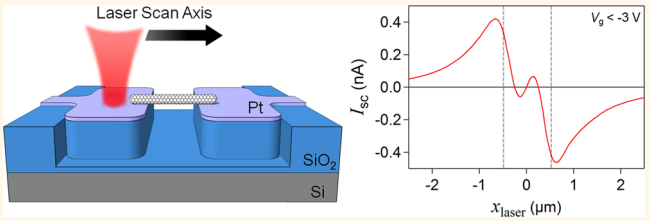

KEYWORDS: suspended carbon nanotubes · field-effect transistors · scanning photocurrent microscopy · photovoltage · photothermoelectric effect · photovoltaic effect · Seebeck coefficient

Nanoscale optoelectronic devices exhibit fascinating physical phenomena and are of increasing interest for applications as photodetectors and energy-harvesting devices.[1−5] Recent observations include multiple electron−hole generation in carbon nanotube (CNT) p−n junctions[2] and ultrasensitive bolometric detection in suspended graphene membranes.[4] Nanoscale confinement of the excited carriers in these systems strongly influences the electron transport and energy relaxation pathways responsible for these novel phenomena. For example, the photocurrent extracted from a graphene p−n junction is not dominated by the photovoltaic effect (as expected for traditional semiconductor devices), but rather by a photothermoelectric (PTE) effect.[6]

Carbon nanotubes offer a unique combination of electron transport and energy relaxation pathways. The band gap of a CNT is widely tunable *via* subtle changes in CNT diameter and chirality.[7] Strong electron−electron interactions in CNTs mean that excitons play an important role in light absorption and energy relaxation. These electron−electron interactions also lead to a strong enhancement in the impact ionization pathway for energy relaxation.[2,8]

Carbon nanotube optoelectronic devices have been studied intensively using electrically driven light emission,[3,9] spectrally resolved photoconductivity and photocurrent,[2,10−14] and spatially resolved photocurrent and photoconductivity.[15−19] Previous studies of surface-bound CNT field-effect transistors (FETs) identified the photovoltaic effect as the mechanism for photocurrent generation at the metal−CNT interface.[16−18] In this work, we have investigated suspended CNT FETs. Suspended CNTs become much hotter than substrate-bound CNTs for a given amount of heat input.[20,21] Therefore, the suspended geometry should promote PTE effects.[22,23] Our measurements of suspended CNTs show that light-induced thermal gradients lead to significant currents, which overwhelm photovoltaic currents in some regimes of electrostatic doping. Our measurements give new insight into the tunable and spatially inhomogeneous Seebeck coefficient of electrostatically gated CNTs and demonstrate a new mechanism for optimizing CNT-based photodetectors and energy-harvesting devices.

RESULTS AND DISCUSSION

Figure 1a shows the geometry of our suspended CNT FET.[24] The CNT was grown on top of the Pt electrodes as the last step of the fabrication process. Raman spectra obtained from the suspended CNTs are free from defect peaks, as shown in the inset of

* Address correspondence to minote@science.oregonstate.edu.

Received for review June 20, 2013 and accepted December 19, 2013.

Published online December 19, 2013
10.1021/nn403137a

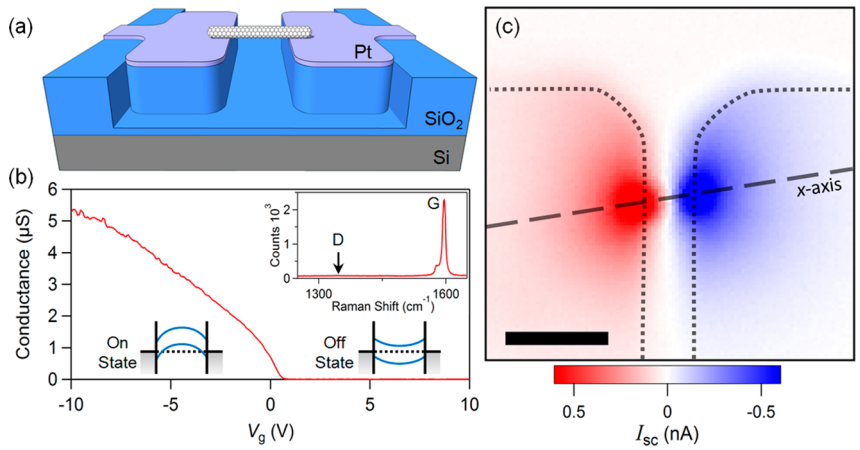

Figure 1. Suspended CNT FET device characteristics. (a) Diagram of suspended nanotube device. (b) Conductance measurement of device 1 taken with a 25 mV source−drain bias voltage. Inset graph shows Raman spectra from the suspended CNT. Inset diagrams show band bending for the on and off states. (c) Short-circuit scanning photocurrent image of device 1 taken with $G(V_g = 0) \approx 1$ μS. Laser power at the sample is 100 μW (λ = 633 nm). Dotted lines represent the electrode edges as measured from corresponding reflectance image (not shown). Dashed line shows CNT axis (*x*-axis). Scale bar is 2 μm.

Figure 1b (in contrast to Raman spectra obtained from surface-bound CNT sections). The absence of a defect peak indicates that the suspended CNT is free from electrostatic disorder.[25] Figure 1b shows a typical low-bias conductance measurement of a completed suspended CNT FET (device 1) where a single CNT connects the electrodes.

The high on/off ratio of the FET (Figure 1b) indicates a band gap greater than about 0.5 eV. For a more accurate estimate of CNT band gap, an additional 10 semiconducting CNT devices were fabricated and tested by spectrally resolved photoconductivity measurements.[10,26] Determination of E_{33} and E_{44} resonances yielded diameters ranging from 1.9 to 2.4 nm. It is somewhat surprising that no CNTs were found with smaller diameters. However, all devices were preselected to have good electrical contact, and it is known that metal/CNT contact improves dramatically with increasing CNT diameter.[27] We conclude that the CNTs in this study have diameters ranging from 1.9 to 2.4 nm and band gaps ranging from 0.73 to 0.58 eV.[28]

A photocurrent image of device 1 is shown in Figure 1c. To make this image, we raster scanned a 100 μW diffraction-limited laser spot, wavelength 633 nm, across the device while recording the short-circuit current I_{sc} as a function of laser position. Electrode edges (dotted lines in Figure 1c) are located by measuring the reflected laser light intensity. From the reflection image, we determine the laser intensity profile follows a Gaussian point spread function with fwhm $\approx$ 550 nm. The photocurrent image shows strong responses where the CNT contacts the metal. A halo of photocurrent extends more than 2 μm away from each CNT−metal contact point. Similar observations of long-range signals have been reported previously.[16,17,23]

To gain more insight into the photocurrent generation mechanisms, we performed line scans of laser position, x_{laser}, along the CNT axis (*x*-axis) at different

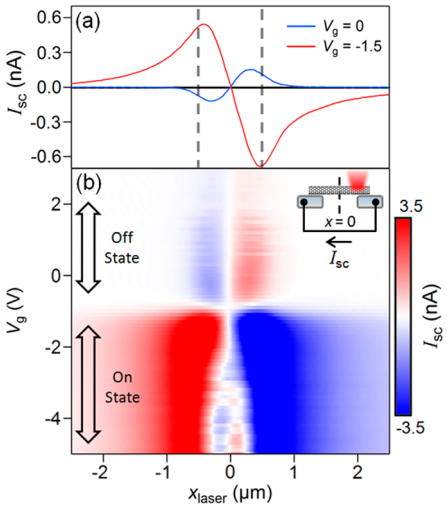

Figure 2. Gate-dependent line scans of device 1. (a) Line scans of I_{sc} measured in the on state ($V_g = -1.5$ V) and off state ($V_g = 0$) taken along the *x*-axis shown in Figure 1c. Vertical dashed lines in (a) indicate the position of the electrode edges. (b) Map of the gate voltage dependence of I_{sc} along the *x*-axis. Laser power at the sample is 120 μW (λ = 633 nm). The center of the trench is defined as $x = 0$. The inset diagram shows the I_{sc} measurement configuration.

values of V_g. The line traces in Figure 2a show $I_{sc}(x_{laser})$ at $V_g = 0$ V (in the off state) and $V_g = -1.5$ V (in the on state). The position $x_{laser} = 0$ corresponds to when the laser is centered on the middle of the trench. The color map of $I_{sc}(x_{laser}, V_g)$ shows the evolution of $I_{sc}(x_{laser})$ as a function of V_g. Understanding the features in $I_{sc}(x_{laser}, V_g)$ is the central topic of this paper.

When the laser spot is centered several micrometers from the electrode edge, the suspended CNT is not illuminated. In this case, current cannot be generated by a photovoltaic mechanism; therefore, we explore the possibility of a PTE effect. Figure 3 shows the open-circuit voltage $V_{oc}(V_g)$ with the laser spot centered at $x \approx 1.8$ μm (illuminating the metal electrode, but not

the CNT). A peak response of $V_{oc} = 250\ \mu V$ is observed at $V_g = 0.3$ V (the threshold of the on state). The polarity of V_{oc} corresponds to a buildup of negative charge on the laser-illuminated electrode or, equivalently, a buildup of positive charge on the dark electrode. The open-circuit voltage falls to a plateau at more negative V_g and drops to near zero at positive V_g.

From previous thermoelectric measurements of single-walled CNT devices,[29] we expect

$$V_{oc} = \bar{S}(V_g)\Delta T \quad (1)$$

where ΔT is the temperature difference across the CNT device, $\bar{S}(V_g) > 0$ is the effective Seebeck coefficient for a p-type CNT device (spatially averaged along the length of the CNT), and the Seebeck coefficient of the metal electrodes is negligible ($S_{Pt}(300\ K) \approx -5\ \mu V/K$).[30] Small *et al.* used on-chip heaters and thermometers to determine $\bar{S}(V_g)$ of nonsuspended semiconducting CNT devices (Figure 3, open circles). Small *et al.* observed a peak value of $\bar{S}(V_g) \approx 250\ \mu V/K$ when V_g was set to the on-state threshold.

When $x_{laser} = 1.8\ \mu m$, we estimate $\Delta T = 1$ K; that is, the hot end of the CNT is 1 K hotter than the cold end. We find this ΔT value *via* two independent approaches. In the first approach, we assume that the previously measured peak Seebeck coefficient, 250 μV/K, is approximately equal for surface-bound and suspended CNTs. In the second approach, we measure the temperature of a CNT on top of a Pt electrode when the CNT and Pt are illuminated by a 100 μW laser. This thermometry measurement is performed by micro Raman spectroscopy and utilizes the temperature-dependent G-band shift. We find a temperature rise of 2 K directly underneath the laser spot and estimate the resulting $\Delta T = 1$ K (see Supporting Information).

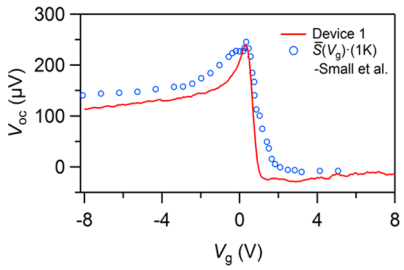

Figure 3. Open-circuit voltage $V_{oc}(V_g)$ generated by device 1 at $x_{laser} = 1.8\ \mu m$. Open circles represent the Seebeck coefficient measurement of a semiconducting CNT from Small *et al.* replotted here for a temperature difference $\Delta T = 1$ K. Small's data have been offset in V_g to match the threshold voltage of device 1.

Figure 3 shows a comparison between our measurement of $\bar{S}(V_g)(1\ K)$ and the previous measurement by Small *et al.* The data are in good agreement if one assumes a factor 2 difference in gate-coupling efficiency. In addition to differences in gate-coupling efficiency, a sharper peak in $V_{oc}(V_g)$ could also be caused by the absence of substrate-induced electrostatic disorder in suspended CNTs.[31]

Returning now to Figure 2, we can understand the gradual increase in on-state I_{sc} as the laser moves closer to the electrode edge. Scanning the laser toward the electrode edge will increase the temperature at the hot end of the CNT, thereby increasing ΔT. The observed rise in $I_{sc}(x_{laser})$ is consistent with a thermally driven I_{sc} that tracks ΔT. The on-state ($V_g < -2$ V) photocurrent peaks at $x_{laser} \approx \pm 0.6\ \mu m$, where the laser spot reaches the edge of the metal electrode.

As the laser begins to illuminate the CNT, light can be absorbed by both the CNT and the metal electrode. To study this mixed regime, it is helpful to identify current generated by CNT absorption as opposed to current generated by heating of the metal electrode. The absorption cross section of the CNT is known to be polarization dependent;[32] therefore, we measured $I_{sc}(V_g, x_{laser})$ with polarization either parallel (∥) (Figure 4a) or perpendicular (⊥) to the CNT axis. Figure 4b shows the difference between the two laser polarization measurements: $\Delta I_{sc}(V_g, x_{laser}) = I_{sc,\parallel}(V_g, x_{laser}) - I_{sc,\perp}(V_g, x_{laser})$.

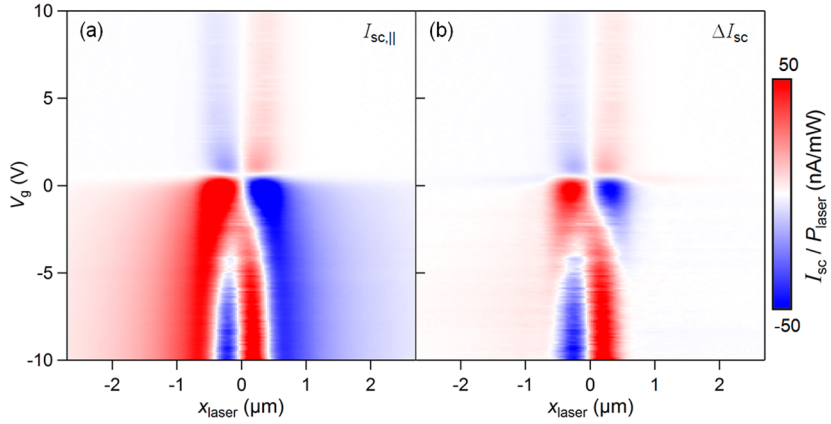

Figure 4. Polarization-dependent photocurrent maps. (a) $I_{sc,\parallel}(V_g, x_{laser})$ and (b) $\Delta I_{sc}(V_g, x_{laser}) = I_{sc,\parallel}(V_g, x_{laser}) - I_{sc,\perp}(V_g, x_{laser})$ from device 2. Photocurrent values have been normalized by the incident laser power, ~70 μW.

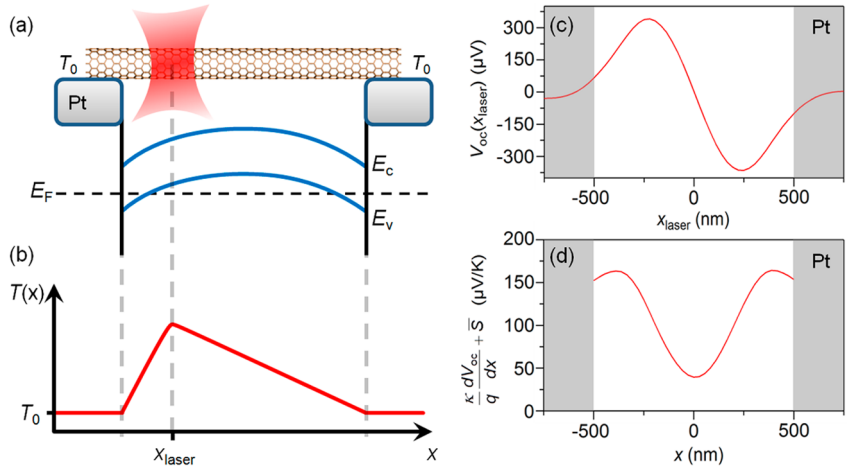

Figure 5. Mechanism for the on-state PTE response. (a) Cartoon of the laser-illuminated device and corresponding on-state band diagram. (b) Temperature profile due to photoinduced heating. The laser is considered to be a point source at x_{laser}. (c) Measured $V_{oc}(x_{laser})$ at $V_g \approx -10$ V after removing contributions from heating of the metal electrodes (Figure 4b). (d) The result of eq 3 calculated using V_{oc} from (c) and $\bar{S} \approx 120$ μV/K.

Figure 4b shows that light absorption by the CNT also plays an important role in photocurrent generation. We first examine the off-state photocurrent, where $I_{sc,\parallel}(V_g, x_{laser}) \approx 3.5 I_{sc,\perp}(V_g, x_{laser})$. The ratio of $I_{sc,\parallel}$ to $I_{sc,\perp}$ is consistent with previous photocurrent polarization ratios for CNTs,[11] and we conclude that $\Delta I_{sc}(V_g, x_{laser})$ corresponds to approximately 70% of the current generated by CNT light absorption. In the off state, the parallel and perpendicular polarization measurements have the same functional form, with Gaussian peaks at ± 0.3 μm (fwhm = 550 nm). These observations show that heating of the metal electrode does not generate photocurrent in the off state. We conclude that the photocurrent observed in the off state is due to the photovoltaic effect, in agreement with previous measurements of surface-bound CNTs.[16−18]

Next we discuss ΔI_{sc} near the transition between off state and on state, which occurs at $V_g \approx 0$ V for this device. Tuning V_g from the off state to the on state leads to an abrupt sign flip in ΔI_{sc} and an increase in the magnitude of ΔI_{sc}. The peaks in $\Delta I_{sc}(x_{laser})$ remain at ± 0.3 μm. This behavior is consistent with the photovoltaic mechanism. First, the sign flip is expected from a reversal of band bending (see diagrams in Figure 1b). Second, the position of the peaks do not shift, indicating the mechanism is the same on both sides of the transition. Third, the change in magnitude is expected due to the asymmetry between the Schottky barriers for n-type/p-type transport. A large barrier limits the extraction of photogenerated electrons in the off state, while a small barrier limits the extraction of photogenerated holes in the on state. We conclude that the ΔI_{sc} signal near the on/off transition is due to the photovoltaic effect.

Deeper in the on state ($V_g < -3$ V) there is another sign flip in ΔI_{sc}. In Figure 4b this is seen as the gradual emergence of peaks at $x_{laser} \approx \pm 0.2$ μm, which overwhelm the peaks at ± 0.3 μm. We have observed these unexpected features in all five devices measured. These anomalous photocurrent features contradict all predictions of the photovoltaic mechanism.

When light is absorbed by the CNT, hot electron−hole pairs are generated. These electron−hole pairs can contribute directly to I_{sc} *via* the photovoltaic mechanism, but they also raise the local temperature of the CNT. In our experiment, the photon energy is approximately 1.5 eV greater than the band gap. Much of this excess energy will be redistributed *via* rapid relaxation pathways such as optical phonon generation and collisions with other charge carriers, both of which occur on the 10 fs time scale.[8] We argue below that this photoinduced heating creates temperature gradients in the CNT, thereby driving PTE currents that dominate ΔI_{sc} at more negative V_g.

Previous authors have quantified the phonon temperature of suspended CNTs while illuminating the CNT with a focused laser.[21] The key factors determining the CNT phonon temperature are the rate that heat is delivered, the distance from the laser-heated segment to the metal electrodes, the thermal conductance of the CNT, and the thermal contact resistance at the CNT−metal contact. On the basis of the results of Hsu *et al.*,[21] a 100 μW laser focused on the CNT a few hundred nanometers from the electrode will heat the CNT by a few Kelvin. For a more accurate estimate we conducted G-band shift thermometry measurements on device 2 (Figure 4) and found a temperature increase at the center of the CNT of $T_{max} - T_0 \approx 5$ K for an incident power of 100 μW, where T_0 is the ambient temperature (see Supporting Information).

Figure 5 shows our proposed mechanism for the new photocurrent peaks emerging at $V_g < -3$ V. The Seebeck coefficient in the CNT will be spatially inhomogeneous due to band bending (Figure 5a). In sections of the CNT that are lightly doped, $S(x)$ will be

large (on the order of 250 μV/K). In sections of CNT that are heavily doped, $S(x)$ will be small. For an inhomogeneous system, the net PTE voltage is found by calculating

$$V_{oc}(x_{laser}) = -\int S(x)\frac{dT(x, x_{laser})}{dx}dx \quad (2)$$

where $T(x,x_{laser})$ the temperature profile along the CNT for a given laser position. For the purpose of calculations, we assume a temperature T_0 at both electrodes (ideal heat sinks) and a triangular peak in the temperature profile (see Figure 5b). With such a temperature profile, eq 2 predicts zero voltage if $S(x)$ is homogeneous, for example, in the flat band condition when the CNT is uniformly doped. However, eq 2 predicts a nonzero V_{oc} as $S(x)$ becomes inhomogeneous. Deep in the on state, $S(x)$ will be large near the electrodes (lightly doped sections of the CNT) and small in the center of the CNT (highly doped sections of the CNT). The polarity of ΔI_{sc} that we observe deep in the on state is consistent with this expected $S(x)$.

To further test this proposed mechanism, we estimate $S(x)$ directly from measurements of $V_{oc}(x_{laser})$ (note that V_{oc} is equal to I_{sc} multiplied by the on-state resistance of the device). We utilize a relationship derived by St. Antoine *et al.* for a 1d system with uniform thermal conductivity κ, heated by a zero-width source that delivers heat at position x at a rate q.[22] For this ideal system, it is found that

$$S(x) = \frac{\kappa}{q}\frac{dV_{oc}}{dx} + \bar{S} \quad (3)$$

The ratio q/κ can be determined from the maximum temperature rise at the center of the CNT. We find $q/\kappa \approx$ 20 K/μm when the laser power is 100 μW.

Figure 5c,d show plots of $V_{oc}(x_{laser})$ and the calculated $S(x)$ when $V_g = -10$ V. The parameter $\bar{S}$ is found from earlier measurements of $\bar{S}(V_g)$ (Figure 3). Consistent with the expected band bending, the calculated $S(x)$ is large near the electrodes and small near the center of the CNT. The calculated $S(x)$ does not reach 250 μV/K (the peak value in Figure 3). However, spatial resolution is limited by the width of the laser spot, and we interpret the calculated $S(x)$ as a locally averaged value. With improved spatial resolution we would expect to reveal narrower/taller peaks in $S(x)$.

The analysis described above could be improved by direct measurement of the electron temperature in the CNT. Raman-shift thermometry, which we use in this work, measures the phonon temperature in the CNT. However, gradients in the electron (or hole) temperature ultimately drive the PTE effect. Photoexcitation does not always heat the electron system and the phonon system equally. For example, in laser-illuminated graphene photodiodes the electron temperature is thought to differ from the phonon temperature.[6] For our CNT devices, the thermal conductivity between the free carriers and the lattice is less than the thermal conductivity from the lattice to the electrodes (see Supporting Information). Therefore, the measured phonon temperature is likely a lower bound on the temperature of the free carriers. Further work is required to establish the actual temperature of the free carriers.

In summary, the PTE mechanism explains our experimental observation of anomalous photocurrent features at $V_g < -3$ V. Moreover, $V_{oc}(x_{laser})$ data combined with temperature calibration data can be used to estimate $S(x)$ with diffraction-limited spatial resolution.

CONCLUSION

We have observed evidence for both the photovoltaic mechanism and the PTE mechanism driving photocurrents in suspended CNT FETs. In the off state, the photovoltaic effect is the dominant mechanism. In the on state, laser heating of the electrodes leads to PTE voltages/currents. Utilizing this electrode heating effect, we have made the first measurement of the gate-dependent Seebeck coefficient for an ultraclean suspended CNT. In the on state, laser heating of the CNT also leads to PTE voltages/currents. These PTE effects dominate photovoltaic effects when band bending creates inhomogeneous $S(x)$. To quantify these PTE effects, we introduced temperature calibration techniques that extend the utility of scanning photocurrent microscopy. Our findings demonstrate the critical role of light-induced heating in suspended CNT optoelectronic systems. These heating effects will play a role in optimizing CNT-based photodetectors and light-harvesting devices.

METHODS

We fabricated devices using standard photolithography techniques. Metal electrodes (Pt/Ti, 100/1 nm thickness) sit on a 1 μm thermally grown oxide layer atop p^+ silicon. The source–drain electrodes situated 1 μm apart act as a shadow mask for the etching of a ~1 μm deep trench in the oxide layer. We then pattern catalyst islands of Fe (Fe/SiO_2/Ti, 1/20/1 nm) on the electrodes a few micrometers from the edge of the trench. CNTs are grown as the last step in the fabrication, resulting in defect-free suspended carbon nanotubes.[25]

The design of our home-built scanning photocurrent microscope has been described previously.[26] Measurements of I_{sc} were made using SRS current preamplifier model SR 570. Measurements of V_{oc} were made using a voltage preamplifier (SRS model SR 560).

Conflict of Interest: The authors declare no competing financial interest.

Acknowledgment. We thank G. Nazin for valuable discussions. This material is based upon work supported by the National Science Foundation under Grant No. 1151369. Sample fabrication

was performed at the MaSC Facility at Oregon State University and the Cornell NanoScale Facility, a member of the National Nanotechnology Infrastructure Network, which is supported by the National Science Foundation (Grant ECCS-0335765).

Supporting Information Available: Decomposing the photocurrent from device 2 into polarization-sensitive and polarization-insensitive components; temperature measurements using the Raman G-band; calculation of the expected laser heating of a suspended CNT; order of magnitude calculation for laser heating of the platinum electrode; and an analysis of the electron and phonon temperatures in a laser-illuminated CNT. This material is available free of charge *via* the Internet at http://pubs.acs.org.

REFERENCES AND NOTES

1. Gabor, N. M. Impact Excitation and Electron-Hole Multiplication in Graphene and Carbon Nanotubes. *Acc. Chem. Res.* **2013**, *46*, 1348–1357.
2. Gabor, N. M.; Zhong, Z. H.; Bosnick, K.; Park, J.; McEuen, P. L. Extremely Efficient Multiple Electron-Hole Pair Generation in Carbon Nanotube Photodiodes. *Science* **2009**, *325*, 1367–1371.
3. Misewich, J. A.; Martel, R.; Avouris, P.; Tsang, J. C.; Heinze, S.; Tersoff, J. Electrically Induced Optical Emission from a Carbon Nanotube FET. *Science* **2003**, *300*, 783–786.
4. Freitag, M.; Low, T.; Avouris, P. Increased Responsivity of Suspended Graphene Photodetectors. *Nano Lett.* **2013**, *13*, 1644–1648.
5. Avouris, P. Graphene and Carbon Nanotubes: Advances and Prospects in Electronics and Photonics. *Abstr. Pap. Am. Chem. Soc.* **2010**, 240.
6. Gabor, N. M.; Song, J. C. W.; Ma, Q.; Nair, N. L.; Taychatanapat, T.; Watanabe, K.; Taniguchi, T.; Levitov, L. S.; Jarillo-Herrero, P. Hot Carrier-Assisted Intrinsic Photoresponse in Graphene. *Science* **2011**, *334*, 648–652.
7. Bachilo, S. M.; Strano, M. S.; Kittrell, C.; Hauge, R. H.; Smalley, R. E.; Weisman, R. B. Structure-Assigned Optical Spectra of Single-Walled Carbon Nanotubes. *Science* **2002**, *298*, 2361–2366.
8. Perebeinos, V.; Avouris, P. Impact Excitation by Hot Carriers in Carbon Nanotubes. *Phys. Rev. B* **2006**, *74*, 121410.
9. Chen, J.; Perebeinos, V.; Freitag, M.; Tsang, J.; Fu, Q.; Liu, J.; Avouris, P. Bright Infrared Emission from Electrically Induced Excitons in Carbon Nanotubes. *Science* **2005**, *310*, 1171–1174.
10. Freitag, M.; Martin, Y.; Misewich, J. A.; Martel, R.; Avouris, P. H. Photoconductivity of Single Carbon Nanotubes. *Nano Lett.* **2003**, *3*, 1067–1071.
11. Qiu, X. H.; Freitag, M.; Perebeinos, V.; Avouris, P. Photoconductivity Spectra of Single-Carbon Nanotubes: Implications on the Nature of Their Excited States. *Nano Lett.* **2005**, *5*, 749–752.
12. Mohite, A.; Lin, J. T.; Sumanasekera, G.; Alphenaar, B. W. Field-Enhanced Photocurrent Spectroscopy of Excitonic States in Single-Wall Carbon Nanotubes. *Nano Lett.* **2006**, *6*, 1369–1373.
13. Lee, J. U.; Codella, P. J.; Pietrzykowski, M. Direct Probe of Excitonic and Continuum Transitions in the Photocurrent Spectroscopy of Individual Carbon Nanotube P-N Diodes. *Appl. Phys. Lett.* **2007**, *90*, 053103.
14. Barkelid, M.; Steele, G. A.; Zwiller, V. Probing Optical Transitions in Individual Carbon Nanotubes Using Polarized Photocurrent Spectroscopy. *Nano Lett.* **2012**, *12*, 5649–5653.
15. Balasubramanian, K.; Fan, Y. W.; Burghard, M.; Kern, K.; Friedrich, M.; Wannek, U.; Mews, A. Photoelectronic Transport Imaging of Individual Semiconducting Carbon Nanotubes. *Appl. Phys. Lett.* **2004**, *84*, 2400–2402.
16. Balasubramanian, K.; Burghard, M.; Kern, K.; Scolari, M.; Mews, A. Photocurrent Imaging of Charge Transport Barriers in Carbon Nanotube Devices. *Nano Lett.* **2005**, *5*, 507–510.
17. Freitag, M.; Tsang, J. C.; Bol, A.; Yuan, D. N.; Liu, J.; Avouris, P. Imaging of the Schottky Barriers and Charge Depletion in Carbon Nanotube Transistors. *Nano Lett.* **2007**, *7*, 2037–2042.
18. Ahn, Y. H.; Tsen, A. W.; Kim, B.; Park, Y. W.; Park, J. Photocurrent Imaging of P-N Junctions in Ambipolar Carbon Nanotube Transistors. *Nano Lett.* **2007**, *7*, 3320–3323.
19. Buchs, G.; Barkelid, M.; Bagiante, S.; Steele, G. A.; Zwiller, V. Imaging the Formation of a P-N Junction in a Suspended Carbon Nanotube with Scanning Photocurrent Microscopy. *J. Appl. Phys.* **2011**, *110*, 074308.
20. Pop, E.; Mann, D.; Cao, J.; Wang, Q.; Goodson, K. E.; Dai, H. J. Negative Differential Conductance and Hot Phonons in Suspended Nanotube Molecular Wires. *Phys. Rev. Lett.* **2005**, *95*, 155505.
21. Hsu, I. K.; Kumar, R.; Bushmaker, A.; Cronin, S. B.; Pettes, M. T.; Shi, L.; Brintlinger, T.; Fuhrer, M. S.; Cumings, J. Optical Measurement of Thermal Transport in Suspended Carbon Nanotubes. *Appl. Phys. Lett.* **2008**, *92*, 063119.
22. St-Antoine, B. C.; Menard, D.; Martel, R. Position Sensitive Photothermoelectric Effect in Suspended Single-Walled Carbon Nanotube Films. *Nano Lett.* **2009**, *9*, 3503–3508.
23. St-Antoine, B. C.; Menard, D.; Martel, R. Photothermoelectric Effects in Single-Walled Carbon Nanotube Films: Reinterpreting Scanning Photocurrent Experiments. *Nano Res.* **2012**, *5*, 73–81.
24. Sharf, T.; Kevek, J. W.; Minot, E. D. In *Fabrication of Low-Noise Carbon Nanotube Field-E□ect Transistor Biosensors*; Nanotechnology (IEEE-NANO); 11th IEEE Conference, Aug 15−18, 2011; **2011**; pp 122−125.
25. Sharf, T.; Kevek, J. W.; DeBorde, T.; Wardini, J. L.; Minot, E. D. Origins of Charge Noise in Carbon Nanotube Field-Effect Transistor Biosensors. *Nano Lett.* **2012**, *12*, 6380–6384.
26. DeBorde, T.; Kevek, J. W.; Sharf, T.; Wardini, J. L.; Minot, E. D. In *A Spectrally-Tunable Photocurrent Microscope for Characterizing Nanoelectronic Devices*; Nanotechnology (IEEE-NANO); 11th IEEE Conference, Aug 15−18, 2011; **2011**; pp 382−386.
27. Kim, W.; Javey, A.; Tu, R.; Cao, J.; Wang, Q.; Dai, H. J. Electrical Contacts to Carbon Nanotubes Down to 1 nm in Diameter. *Appl. Phys. Lett.* **2005**, *87*, 173101.
28. Dukovic, G.; Wang, F.; Song, D. H.; Sfeir, M. Y.; Heinz, T. F.; Brus, L. E. Structural Dependence of Excitonic Optical Transitions and Band-Gap Energies in Carbon Nanotubes. *Nano Lett.* **2005**, *5*, 2314–2318.
29. Small, J. P.; Perez, K. M.; Kim, P. Modulation of Thermoelectric Power of Individual Carbon Nanotubes. *Phys. Rev. Lett.* **2003**, *91*, 256801.
30. Moore, J. P.; Graves, R. S. Absolute Seebeck Coefficient of Platinum from 80 to 340 K and Thermal and Electrical Conductivities of Lead from 80 to 400 K. *J. Appl. Phys.* **1973**, *44*, 1174–1178.
31. Amer, M. R.; Bushmaker, A.; Cronin, S. B. The Influence of Substrate in Determining the Band Gap of Metallic Carbon Nanotubes. *Nano Lett.* **2012**, *12*, 4843–4847.
32. Islam, M. F.; Milkie, D. E.; Kane, C. L.; Yodh, A. G.; Kikkawa, J. M. Direct Measurement of the Polarized Optical Absorption Cross Section of Single-Wall Carbon Nanotubes. *Phys. Rev. Lett.* **2004**, *93*, 037404.